

Multi-Source Fusion and Automatic Predictor Selection for Zero-Shot Video Object Segmentation

Xiaoqi Zhao
zxq@mail.dlut.edu.com
Dalian University of Technology
Dalian, Liaoning, China

Youwei Pang
lartpang@mail.dlut.edu.com
Dalian University of Technology
Dalian, Liaoning, China

Jiaxing Yang
jx.yang@mail.dlut.edu.com
Dalian University of Technology
Dalian, Liaoning, China

Lihe Zhang*
zhanglihe@dlut.edu.com
Dalian University of Technology
Dalian, Liaoning, China

Huchuan Lu
lhchuan@dlut.edu.com
Dalian University of Technology
Dalian, Liaoning, China
Pengcheng Lab
Shenzhen, Guangdong, China

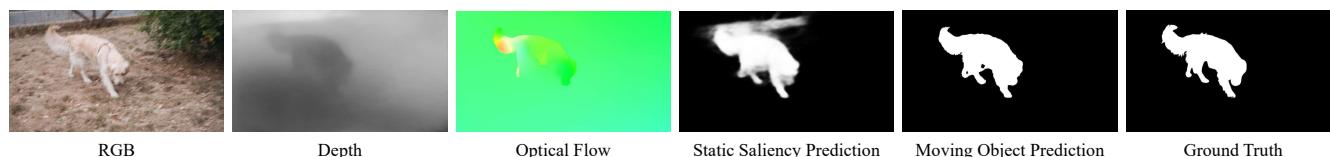


Figure 1: Visual results of different sources.

ABSTRACT

Location and appearance are the key cues for video object segmentation. Many sources such as RGB, depth, optical flow and static saliency can provide useful information about the objects. However, existing approaches only utilize the RGB or RGB and optical flow. In this paper, we propose a novel multi-source fusion network for zero-shot video object segmentation. With the help of interoceptive spatial attention module (ISAM), spatial importance of each source is highlighted. Furthermore, we design a feature purification module (FPM) to filter the inter-source incompatible features. By the ISAM and FPM, the multi-source features are effectively fused. In addition, we put forward an automatic predictor selection network (APS) to select the better prediction of either the static saliency predictor or the moving object predictor in order to prevent over-reliance on the failed results caused by low-quality optical flow maps. Extensive experiments on three challenging public benchmarks (i.e. DAVIS₁₆, Youtube-Objects and FBMS) show that the proposed model achieves compelling performance against the state-of-the-arts. The source code will be publicly available at <https://github.com/Xiaoqi-Zhao-DLUT/Multi-Source-APS-ZVOS>.

*Corresponding author.

Permission to make digital or hard copies of all or part of this work for personal or classroom use is granted without fee provided that copies are not made or distributed for profit or commercial advantage and that copies bear this notice and the full citation on the first page. Copyrights for components of this work owned by others than ACM must be honored. Abstracting with credit is permitted. To copy otherwise, or republish, to post on servers or to redistribute to lists, requires prior specific permission and/or a fee. Request permissions from permissions@acm.org.

MM '21, October 20–24, 2021, Virtual Event, China

© 2021 Association for Computing Machinery.

ACM ISBN 978-1-4503-8651-7/21/10...\$15.00

<https://doi.org/10.1145/3474085.3475192>

CCS CONCEPTS

• Computing methodologies → Video segmentation.

KEYWORDS

Video Object Segmentation, Multi-source Information, Interoceptive Spatial Attention, Feature Purification, Predictor Selection

ACM Reference Format:

Xiaoqi Zhao, Youwei Pang, Jiaxing Yang, Lihe Zhang, and Huchuan Lu. 2021. Multi-Source Fusion and Automatic Predictor Selection for Zero-Shot Video Object Segmentation. In *Proceedings of the 29th ACM International Conference on Multimedia (MM '21)*, October 20–24, 2021, Virtual Event, China. ACM, New York, NY, USA, 9 pages. <https://doi.org/10.1145/3474085.3475192>

1 INTRODUCTION

Zero-shot video object segmentation (ZVOS) aims to automatically separate primary foreground object/objects from their background in a video without any human annotation for testing frames. It has attracted a lot of interests due to the wide application scenarios such as autonomous driving, video surveillance and video editing. With the development of deep convolutional neural networks (CNNs), the CNNs-Based ZVOS methods dominate this field. According to the way of capturing the moving objects, ZVOS methods can be divided into interframe-based [6, 20, 38, 45, 48, 51] and optical flow based methods [2, 41, 56, 59]. In this paper, we utilize the optical flow to depict motion information of video objects.

To achieve accurate video object segmentation, the input information sources are important. As we know, a video sequence is made up of a series of static images. The process of observing objects is from static to dynamic. If the object in a video no longer moves or moves very slowly, its segmentation is converted to a

static salient object segmentation problem. When there is obvious relative motion in the scene, the optical flow map contains the patterns of objects, surfaces and edges. In addition, the depth map can also provide useful complementary information for segmentation tasks, such as temporal action localization [13], RGB-D semantic [18, 46, 53] and saliency segmentation [25, 54, 57]. Thus, the RGB, optical flow, depth and static saliency all can provide the vital position and appearance cues about video objects, and each source has the complementarity, as shown in Fig. 1.

However, all previous ZVOS methods only focus on the RGB or RGB and optical flow, other sources are neglected. Besides, existing optical flow based approaches extremely rely on the optical flow at multiple levels. If the foreground (object) shifts significantly, the optical flow map can capture the object well, which is beneficial to the network. On the contrary, if the background changes drastically or the foreground hardly moves, the resulted optical flow may be noise for ZVOS. As shown in Fig. 2, the high-quality optical flow can provide effective guidance, while the low-quality one easily brings the interference. How to avoid this problem is not considered by previous optical flow based methods.

Motivated by these observations, we propose a novel multi-source fusion and automatic predictor selection network. Firstly, we design a simple multi-task network, which aims to predict the depth map and static saliency map from RGB image. It adopts the FPN [17] structure with one encoder and two decoders. The encoder extracts the RGB features, while the decoders infer the depth and static saliency features, respectively. Secondly, we design an interoceptive spatial attention module (ISAM) to effectively combine the feature maps provided by four kinds of sources (i.e, RGB, depth, optical flow and static saliency). The ISAM can adaptively perceive the importance of each source features in their spatial positions compared to other sources, thereby preserving the source-specific information in the fused features. Since multiple sources contain some mutual interference effects, we build a feature purification module (FPM) to filter out the incompatible information. With the help of ISAM and FPM, the moving object can be segmented precisely. Lastly, we design an automatic predictor selection network (APS) to evaluate the objectness of the optical flow and choose the result between static salient object segmentation and moving object segmentation, thereby avoiding the prediction failure caused by the optical flow.

Our main contributions can be summarized as follows:

- We present a novel solution and new insight for zero-shot video object segmentation by utilizing multiple sources to provide comprehensive location and appearance information of video objects.
- We design an interoceptive spatial attention module (ISAM) and a feature purification module (FPM) to obtain multi-source compatible features.
- We propose an automatic predictor selection network to adaptively choose better prediction from either the static saliency predictor or the moving object predictor.
- Experimental results indicate that the proposed method significantly surpasses the existing state-of-the-art algorithms on three popular ZVOS benchmarks DAVIS₁₆, Youtube-Objects and FBMS.

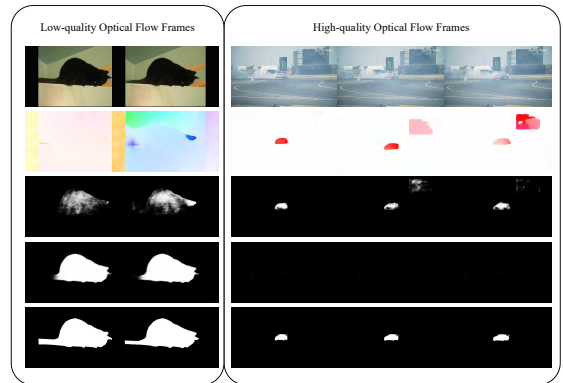


Figure 2: Visual results of static and motion prediction.

2 RELATED WORK

2.1 Zero-shot Video Object Segmentation

Different from one-shot video object segmentation (OVOS), ZVOS aims to automatically detect the target object without any human definition. Many CNNs-based methods [6, 20, 37, 38, 45, 48] are proposed to utilize the inter-frame relationship to capture rich context and enable a more complete understanding of video content. For instance, recurrent neural network is used to capture temporal information in [38, 48]. Lu *et al.* [20] take a pair of frames as input and learn their correlations by using co-attention mechanism. Wang *et al.* [45] propose an attended graph neural network and perform recursive message passing to mine the underlying high-order correlations.

In addition, optical flow itself can provide important motion information. Benefiting from some outstanding optical flow estimation methods [39, 40, 55], optical flow map can be easily obtained and applied to ZVOS. Tokmakov *et al.* [41] only use the optical flow map as the input and build a fully convolutional network to segment the moving object. But this map can not provide sufficient appearance information compared to the RGB input. In [2, 16, 42, 59], two parallel streams are built to extract features from the RGB image and optical flow map, which are further fused in the decoder to predict the segmentation results. The MATNet [59] achieves the transition of attended motion features to enhance appearance learning at each convolution stage. However, the aforementioned optical flow based methods depend on the optical flow map heavily. This map deeply participates in the feature fusion of the network. Once its quality is very low, it is bound to result in very serious interference. To address this issue, we put forward an automatic predictor selection network to judge the effectiveness of the optical flow based predictor.

2.2 Multi-source Information

The RGB refers to three channels of red, green and blue. This standard includes almost all colors that human vision can perceive, and is one of the most widely used color systems. Many computer vision tasks, such as classification, object detection, object tracking and semantic segmentation all use the RGB image as the main input source. However, only relying on the RGB source is difficult to handle some complex environments such as low-contrast objects,

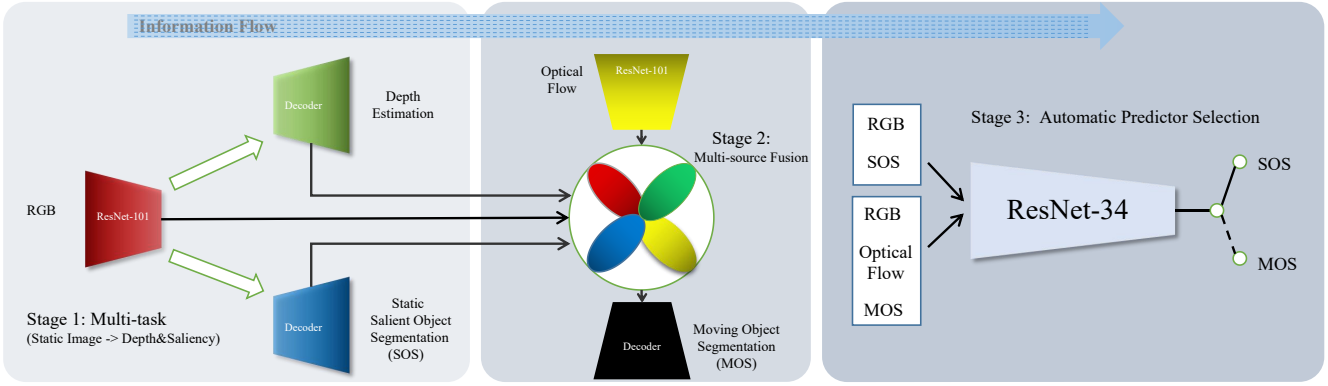


Figure 3: Network pipeline of the ZVOS task. It consists of three stages: multi-task prediction, multi-source fusion and automatic predictor selection. The first stage network is used to generate features of RGB, depth and static saliency. The interoceptive spatial attention module (ISAM) and the feature purification module (FPM) are equipped in the second stage network to achieve multi-source fusion. The third stage network selects a better prediction from either the static object predictor or moving object predictor as the final output.

which share similar appearances to the background. Benefiting from Microsoft Kinect and Intel RealSense devices, depth information can be conveniently obtained. Moreover, the stable geometric structures depicted in the depth map are robust against the changes of illumination and texture, which can provide important supplementary information for handling complex scenarios. Therefore, many RGB-D methods are applied in different tasks, such as RGB-D semantic segmentation, RGB-D salient object segmentation, and RGB-D tracking [1, 21, 36].

In addition, as an important computer vision task, salient object segmentation also needs to delineate the location and contour information of salient objects in a scene, which can provide crucial cues for ZVOS. Many methods [10, 33, 56] are proposed to solve this basic vision task. For the video related task, motion information is a key attribute. How to effectively capture motion prior has received much attention, where optical flow estimation is an active research branch. Recently, many CNNs-based methods [11, 35, 39, 50] utilize iterative refinement strategy to improve the performance of optical flow. In this work, we aim to exploit the aforementioned multiple sources to solve the zero-shot video object segmentation.

3 METHODOLOGY

Overall, we segment objects of both motion and appearance saliency within video frames by employing a three-stage pipeline, as shown in Fig. 3. In the first stage, a network capable of achieving simultaneously depth estimation and static salient object segmentation (SOS) is built, which only feeds on static images. In the second, a network able to fuse features from different sources (RGB image, depth, static saliency, and optical flow) is engineered to achieve moving object segmentation (MOS), with an interoceptive spatial attention module (ISAM) and a feature purification module (FPM) at its core. In the third, a discriminator network is applied to judge SOS and MOS outputs according to their respective confidence scores, to self-adaptively decide which is the desirable one. The

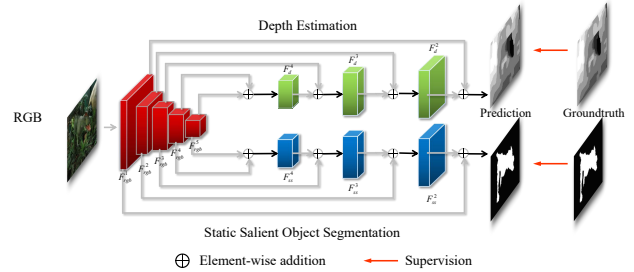


Figure 4: Illustration of the Multi-task network.

following content will detail the specifics of the three stages in order and show how these specified networks are coordinated.

3.1 Multi-task Prediction

The multi-task network in this stage (adjusted from feature pyramid networks [17]) has a uniencoder-bidecoder structure, as illustrated in Fig. 4, in which the encoder is fed with static images and the decoders will predict depth and static saliency maps, respectively. The encoder uses tail-cast ResNet-101 [9] to accommodate the requirement of our task (fully-convolutional). The two-stream decoders have five upsampling stages to gradually restore resolution of the embedding, during which the features from each encoder stage are fused into their corresponding decoder stages via the self-explaining skip-connection. In addition, we apply foreground object ground truth and depth annotation to supervise their outputs, respectively. For depth stream, we follow the related works [23, 31, 34] to adopt the combination loss of L1 and SSIM [49]. For another, we use BCE loss [4] as in [10, 26, 44, 52, 56]. Such double supervision strategy will drive the transformation of source semantics, namely, RGB source to depth source and static saliency source. Note that compared to the methods directly adopting existing depth estimation and saliency detection networks, our multi-task design will save training and inference time and a number of parameters.

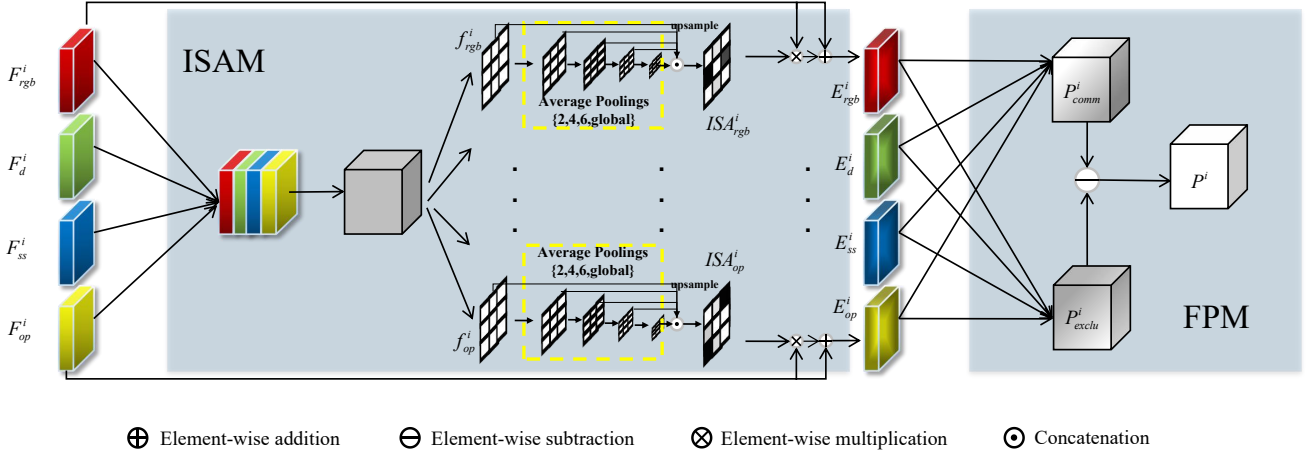


Figure 5: Detailed diagram of interoceptive spatial attention module (ISAM) and feature purification module (FPM).

To be specific, our multi-task network will produce: (1) the RGB feature map F_{rgb}^i ($i \in \{1, 2, 3, 4, 5\}$) which is extracted from the i th level of the encoder; (2) the depth feature map F_d^i from the decoder of depth estimation; (3) the static saliency feature map F_{ss}^i from the decoder of salient object segmentation; (4) the depth map and the static saliency map M_{sos} . The above three kinds of feature maps will be fed into the second stage network together for moving object segmentation.

3.2 Multi-source Fusion

The multi-source fusion network consists of ISAM, FPM, an encoder, and a decoder, as shown in Fig. 3. The encoder and decoder are similar to their counterparts in the first stage. Note that the encoder in this stage is only used to extract motion feature maps F_{op}^i from optical flow map, which is calculated by feeding temporal close frames into the off-the-shelf RAFT Net [40]. Thus, the features of the four sources are well-prepared. The ISAM enhances the spatial saliency of the feature maps of the sources by computing four attention maps. The FPM calculates the difference between features containing inter-source common information and mutually-exclusive information to filter out incompatible contexts. Their internal structures are shown in Fig. 5.

Within the network, ISAM first concatenates all the source feature maps to generate a single-channel interoceptive feature map for each source, as follows:

$$f_{src}^i = Conv_1(Conv_{256}(Cat(F_{rgb}^i, F_d^i, F_{op}^i, F_{ss}^i))), \quad (1)$$

where $src \in \{rgb, d, op, ss\}$ describes the identities of RGB image source, depth source, optical flow source, and static saliency source, respectively. The $Conv_{256}(\cdot)$ and $Conv_1(\cdot)$ operations refer to the 3×3 convolutions with 256 output channels and one output channel, respectively, by which the independent source features are correlated. $Cat(\cdot)$ is the concatenation operation along channel axis. Then, we compute an interoceptive attention map with multi-scale information. This process is formulated as follows:

$$ISA_{src}^i = Sig(Conv_1(Cat(Up(MP(f_{src}^i)))), \quad (2)$$

where MP denotes a group of pooling operations along the channel dimension with scale $\{2, 4, 6, global\}$, $Up(\cdot)$ is the bilinear interpolation to upsample the features map to the same size as f_{src}^i and $Sig(\cdot)$ is the element-wise sigmoid function. The ISA_{src}^i is used to enhance each source feature as follows:

$$E_{src}^i = F_{src}^i + F_{src}^i \otimes ISA_{src}^i, \quad (3)$$

where \otimes represents element-wise multiplication, and E_{src}^i is the enhanced feature at the i th level.

Following ISAM, FPM at every level takes the concatenation of E_{src}^i from different sources as inputs to obtain the fused feature. There is the incompatibility problem when fusing multi-source features. Direct combination P_{comm}^i is not sufficient to dilute incompatible components. Therefore, we construct an auxiliary feature, namely P_{exclu}^i . The fusion process is formulated as:

$$P^i = P_{comm}^i - P_{exclu}^i \quad (4)$$

where P_{comm}^i and P_{exclu}^i can be represented as:

$$\begin{aligned} P_{comm}^i &= Conv_{256}(Cat(E_{rgb}^i, E_d^i, E_{op}^i, E_{ss}^i)), \\ P_{exclu}^i &= Conv_{256}(Cat(E_{rgb}^i, E_d^i, E_{op}^i, E_{ss}^i)). \end{aligned} \quad (5)$$

P_{comm}^i and P_{exclu}^i have different convolution parameters although their formulas are the same. The rationale behind FPM is that the subtraction and the MOS-used supervision will force features P_{comm}^i and P_{exclu}^i to represent the common and mutually-exclusive contexts of the four sources, respectively. After preparing P^i at each level, we gradually combine all of them to generate the final prediction M_{mos} of moving object segmentation by the plain decoder.

3.3 Automatic Predictor Selection

In the third stage, the proposed automatic predictor selection network (APS) will judge which of the outputs from SOS and MOS is more convincing, according to a score. As shown in Fig. 6, the overall network is constructed to solve a binary classification problem. We adopt a lightweight ResNet-34 [9] network in order to reduce the amount of parameters and also for easier training. During the

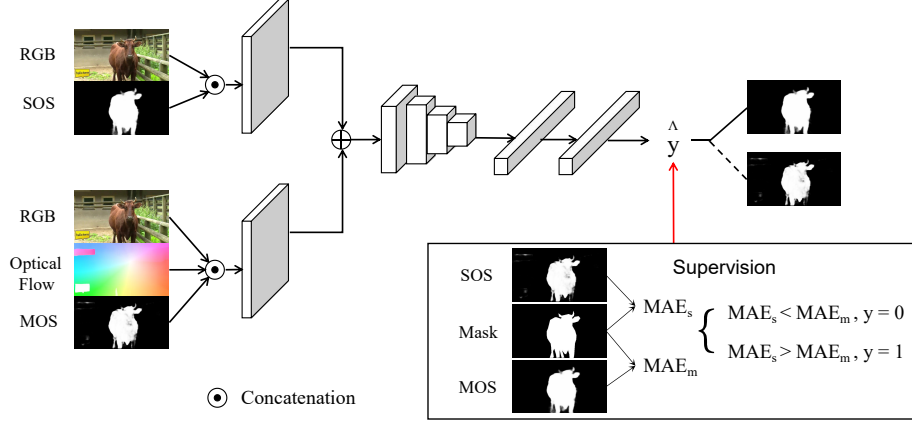


Figure 6: The overall architecture of the automatic predictor selection network.

forward propagation, two inputs are required: (1) the concatenation of RGB and the SOS result; (2) the concatenation of RGB, optical flow map and the MOS result. For mathematical tractability, we use rs and rm to represent them, respectively. We replace the first layer of the encoder with the convolution of 64 output channels, so that it can perceive the two inputs of different sizes. We initialize the parameters of the added convolutional layers with He’s method [8]. After the first layer, we integrate the two-stream feature outputs by element-wise addition. The fused feature maps are fed into the other layers of ResNet-34 pretrained on ImageNet [5], to alleviate the over-fitting problem to some extent. The process of the score prediction can be formulated as follows:

$$\hat{y} = APS(rs, rm; \theta), \quad (6)$$

where θ is the learnable parameters and \hat{y} is the score. To sharp the discrimination ability of APS, we utilize the MAE score to dynamically generate the annotation y :

$$\begin{cases} \mathcal{M}(M_{sos}, G) < \mathcal{M}(M_{mos}, G), y = 0 \\ \mathcal{M}(M_{sos}, G) \geq \mathcal{M}(M_{mos}, G), y = 1, \end{cases} \quad (7)$$

where \mathcal{M} is the MAE defined as the average pixel-wise absolute difference between the prediction M and ground-truth G :

$$MAE = \frac{1}{W \times H} \sum_{w=1}^W \sum_{h=1}^H (M(w, h) - G(w, h)), \quad (8)$$

where W, H are the width and height of the ground-truth mask, respectively. Finally, we adopt the binary cross entropy loss, which can be computed as:

$$\mathcal{L}_{bce} = -(y \log \hat{y} + (1 - y) \log(1 - \hat{y})). \quad (9)$$

Supervised by the dynamic binary classification annotation, the APS network can learn the predictor selection rule that a lower score represents a higher confidence of the SOS and a lower degree of matching among MOS, optical flow and RGB. On the contrary, a higher score means a higher confidence of the MOS and a lower degree of matching between SOS and RGB. Therefore, the APS network implements the function of evaluating the effectiveness of object-information contained in the optical flow for ZVOS.

4 EXPERIMENTS

4.1 Datasets and Evaluation Metrics

DAVIS₁₆ [29] is one of the most popular benchmark datasets for video object segmentation task. It consists of 50 high-quality video sequences (30 for training and 20 for validation) in total. And most videos do not have special scenes such as dramatic changes in the background or almost no movement in the foreground. Usually, the high-quality optical flow map can be obtained via optical flow networks. We use two standard metrics: mean similarity \mathcal{J} and mean boundary accuracy \mathcal{F} [29] to measure the segmentation results (The higher are better).

Youtube-Objects [32] is a large dataset of 126 web videos with 10 semantic object categories and more than 20,000 frames. This dataset contains many unconventional videos, such as dramatically-changing backgrounds, slowly-moving or stationary objects, objects only moving in the depth dimension. The quality of optical flow map is usually low in these video sequences. Following most methods [20, 38, 45, 48, 51, 59], we only use the mean region similarity \mathcal{J} metric to measure the performance.

FBMS [24] is composed of 59 video sequences with ground truth annotations provided in a subset of the frames. Following the standard protocol [42] and other methods [38, 59], we do not use any sequences within for training and only evaluate on the validation set, which consists of 30 sequences. Since it is designed for their specific purposes, FBMS is not often used for the ZVOS task. We just use it for a fair comparison.

4.2 Implementation Details

Our model is implemented based on Pytorch and trained on a PC with an RTX 2080Ti GPU. The input sources are all resized to 384×384 and all the three stages use the mini-batch of size 4 for training. First, we use some RGB-D saliency datasets [3, 7, 14, 22, 28, 30] to train the multi-task network. Once the first stage training is finished, we adopt the DAVIS₁₆ training set to train the multi-source fusion network. In the process, the parameters of the multi-task network is frozen, and we just train the multi-source fusion network. We use a total of 8,363 labeled samples including video data (2,000 + frames)

Table 1: Quantitative comparison on the DAVIS₁₆ [29] validation set. The best result for each metric is red. All the results are borrowed from the public leaderboard maintained by the DAVIS challenge or the corresponding papers.

Methods	Interframe-based methods								Optical flow-based methods				
	PDB [38]	MotAdapt [37]	EPO [6]	AGS [48]	COSNet [20]	AGNN [45]	DFNet [58]	WCS [51]	SFL [2]	MP [41]	GateNet [56]	MATNet [59]	Ours ours
mean $\mathcal{J} \uparrow$	77.2	77.2	80.6	79.7	80.5	80.7	80.4	82.2	67.4	70.0	80.9	82.4	83.3
mean $\mathcal{F} \uparrow$	74.5	77.4	75.5	77.4	79.5	79.1	–	80.7	66.7	65.9	79.4	80.7	82.1

Table 2: Quantitative results of each category on the Youtube-Objects [32] in terms of mean \mathcal{J} . We show the average performance for each of the 10 categories, and the final row gives an average over all the videos.

	Airplane (6)	Bird (6)	Boat (15)	Car (7)	Cat (16)	Cow (20)	Dog (27)	Horse (14)	Motorbike (10)	Train (5)	Avg.
FST [27]	70.9	70.6	42.5	65.2	52.1	44.5	65.3	53.5	44.2	29.6	53.8
COSEG [43]	69.3	76.0	53.5	70.4	66.8	49.0	47.5	55.7	39.5	53.4	58.1
ARP [15]	73.6	56.1	57.8	33.9	30.5	41.8	36.8	44.3	48.9	39.2	46.2
LVO [42]	86.2	81.0	68.5	69.3	58.8	68.5	61.7	53.9	60.8	66.3	67.5
PDB [38]	78.0	80.0	58.9	76.5	63.0	64.1	70.1	67.6	58.3	35.2	65.4
FSEG [12]	81.7	63.8	72.3	74.9	68.4	68.0	69.4	60.4	62.7	62.2	68.4
AGS [48]	87.7	76.7	72.2	78.6	69.2	64.6	73.3	64.4	62.1	48.2	69.7
COSNet [20]	81.1	75.7	71.3	77.6	66.5	69.8	76.8	67.4	67.7	46.8	70.5
AGNN [45]	81.1	75.9	70.7	78.1	67.9	69.7	77.4	67.3	68.3	47.8	70.8
WCS [51]	81.8	81.2	67.6	79.5	65.8	66.2	73.4	69.5	69.3	49.7	70.9
SFL [2]	65.6	65.4	59.9	64.0	58.9	51.1	54.1	64.8	52.6	34.0	57.0
MATNet [59]	72.9	77.5	66.9	79.0	73.7	67.4	75.9	63.2	62.6	51.0	69.0
Ours	89.4	83.7	75.6	80.7	72.8	71.6	78.8	70.7	63.1	62.2	74.9

Table 3: Quantitative results on the FBMS [24] dataset.

Methods	ARP [15]	SAGE [47]	LVO [42]	FSEG [12]	PDB [38]	MATNet [59]	Ours ours
mean $\mathcal{J} \uparrow$	59.8	61.2	65.1	68.4	74.0	76.1	76.7

and RGB-D SOD data (6300 + images) in the first and second phases. The depth map is obtained by the depth camera. MATNet [59] uses video data (14,000 + frames) for training. AGS [48] uses video data (8,500 + frames) and RGB SOD data (6,000 + images) for training. COSNet [20], AGNN [45] and GateNet [56] use video data (2,000 + frames) and RGB SOD data (15,000 + images). In addition, we expect that there are low-quality and high-quality optical flow videos for training in the third stage, while almost all of the optical flow maps in the DAVIS₁₆ dataset are high-quality, it is not suitable for this training. Therefore, we use 4,000 + frames from the DAVSOD dataset to train the APS. In the inference process, we generate the binary classification using the threshold value of 0.5. In a word, the scale of the used annotations in our training phase is comparable to that of these competitors.

We adopt some data augmentation techniques in each stage to avoid over-fitting: horizontally random flip, random rotate, random brightness, saturation and contrast. For the optimizers, we all use the SGD with a momentum of 0.9 and a weight decay of 0.0005. The learning rate is set to 0.005 and later use the “poly” policy [19] with the power of 0.9 as a means of adjustment.

4.3 Comparison with State-of-the-art

Performance on DAVIS₁₆. We compare the proposed method with the state-of-the-art ZVOS methods on the DAVIS₁₆ benchmark [29]. Tab. 1 shows performance comparison results in terms

of the mean \mathcal{J} and mean \mathcal{F} . It can be seen that ours can consistently outperforms other approaches under the two metrics. Compared to the second best & the optical flow-based method (MATNet), our method achieves an important improvement of 1.1% and 1.7% in terms of mean \mathcal{J} and mean \mathcal{F} , respectively. Moreover, we test the FLOPs of Ours vs. MATNet is 89.6G vs. 120.5G. Therefore, our method has significant advantages in terms of accuracy and computational complexity.

Performance on Youtube-Objects. Tab. 2 shows the results on Youtube-Objects. It can be seen that our method achieves the best performance in eight of the ten categories. Notably, our method has a significant performance improvement of 8.6% in terms of mean \mathcal{J} compared to the optical flow-based method MATNet (74.9 vs. 69.0). As mentioned by Zhou *et al.* [59], Youtube-Objects has many video sequences containing slowly moving and/or visually indistinct objects. Both will result in inaccurate estimation of optical flow. Therefore, the existing optical flow based methods can not perform very well on this dataset. With the help of our automatic predictor selection network, this problem can be solved well.

Performance on FBMS. In order to make a comprehensive comparison with the previous methods, we also show the results on FBMS, as shown in Tab. 3. Our method still achieves the best performance compared to the others.

Qualitative Results. Fig. 7 illustrates visual results of the proposed algorithm on the challenge video sequences *breakdance*, *libby*, *horse jump – high* and *parkour* of DAVIS₁₆. We can see that each source provides rich location and appearance information. Moreover, depth map can supplement extra contrast information,



Figure 7: Qualitative results on four sequences *breakdance*, *libby*, *horse jump – high* and *parkour* of DAVIS₁₆.

Table 4: Ablation study on the validation set of DAVIS₁₆.

Components	Module	mean \mathcal{J}	mean \mathcal{F}
Multi-source feature inputs	RGB	69.2	66.7
	RGB+D	72.5	69.0
	RGB+SOS	72.9	69.3
	RGB+OF	77.3	76.8
	RGB+D+SOS+OF	80.8	80.1
Multi-source fusion	+ISAM	82.5	81.4
	+FPM	83.4	82.3
Prediction	+APS	83.3	82.1

and the high-quality optical flow can provide clear motion information. Notably, none of these sources can dominate the final prediction, and all of the source characteristics must be integrated to achieve high-precision video object segmentation.

4.4 Ablation Study

In this section, we detail the contribution of each component to the overall network. Because the optical flow maps always are high quality on the DAVIS₁₆. We perform an ablation study on it to investigate the effect of multi-source fusion. Specifically, we first verify the effectiveness of each source for moving object segmentation (MOS). Next, we show the benefits of ISAM and FPM in the multi-source fusion network, respectively. Finally, we evaluate the performance of the automatic predictor selection (APS) on both DAVIS₁₆ and Youtube-Objects.

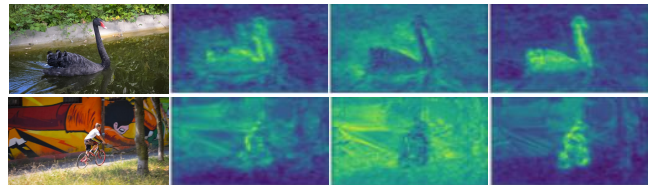


Figure 8: Visual results of p^i_{comm} , p^i_{exclu} and p^i for showing the effect of the feature purification module.

Effectiveness of Multi-source Features. We quantitatively show the benefit of each source in Tab. 4. We take the FPN with the only RGB feature inputs as the baseline. First, the depth features, static saliency features and optical flow features are added to the baseline network, respectively. It can be seen that the combination of RGB source and other sources has a significant improvement compared to the baseline, with the gain of 16.8% and 20.1% in terms of mean \mathcal{J} and mean \mathcal{F} . In the process, multi-source features complement each other without repulsion.

Effectiveness of Multi-source Fusion. We verify the effectiveness of ISAM and FPM in multi-source feature fusion, as shown in Tab. 4. Compared to directly concatenating multi-source feature maps, the ISAM achieves an improvement of 2.1% and 1.6% in terms of mean \mathcal{J} and mean \mathcal{F} . By further equipping the FPM, it can yield continuous performance improvement of 1.1% and 1.1% in terms of mean \mathcal{J} and \mathcal{F} , respectively (finally obtaining a total of 83.4 and 82.3, respectively). To explain the FPM mechanism intuitively, we

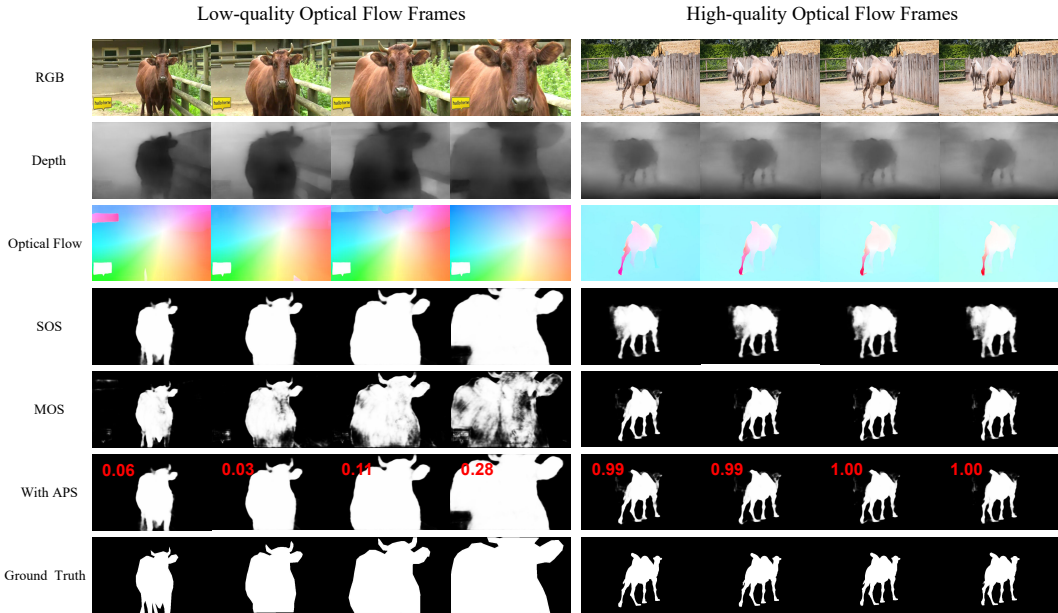


Figure 9: Qualitative results on two example videos *cow* (low-quality optical flow) and *camel* (high-quality optical flow), which are from Youtube-Objects and DAVIS₁₆, respectively.

Table 5: Evaluation of the APS network on both DAVIS₁₆ and Youtube-Objects in terms of mean \mathcal{J} .

Prediction	Youtube-Objects	DAVIS ₁₆
SOS	72.7	67.7
MOS	70.2	83.4
APS	74.9	83.3

visualize some features in Fig. 8. It can be seen that the moving objects in P_{comm}^i are disturbed by much background information, whereas P_{exclu}^i can perspective the background region well. Their subtraction in the FPM actually builds a kind of information constraint by diverse parameters, thereby guaranteeing that P^i can focus on moving objects.

Effectiveness of Automatic Predictor Selection. In Tab. 5, we detail the performance comparison of using APS network on the Youtube-Objects and DAVIS₁₆ datasets, respectively. With the help of high-quality optical flow map, the MOS evidently outperforms the SOS on the DAVIS₁₆. On the contrary, the low-quality optical flow on the Youtube-Objects encumbers the prediction of the MOS, that is, they are not as good as those of SOS. The designed APS network comprehensively evaluates the degree of interference of optical flow to the MOS. It can be seen that our three-stage solving strategy significantly outperforms either of the stand-alone SOS or MOS on the Youtube-Objects. This indicates that the APS is not partial to either of them and has learned the selection mechanism. In addition, the results discriminated by the APS have slightly less mean \mathcal{J} (0.01) on the DAVIS₁₆ than those generated only by MOS, demonstrating that the discriminator in most times will accept the results assisted with high-quality optical flow maps. To more intuitively show the effectiveness of the APS, we visualize all

sources and the results of each stage under optical flow maps of various quality in Fig. 9. It can be observed that the APS tends to give low scores to the video sequences with low-quality optical flow and high scores to the video sequences with high-quality optical flow, respectively.

5 CONCLUSION

In this paper, we propose a novel multi-source fusion network to effectively utilize the complementary features from the RGB, depth, static saliency and optical flow for zero-shot video object segmentation. The proposed interoceptive spatial attention module can adaptively enhance the feature representation of each source in spatial position. With the help of feature purification module, it can further filter the incompatible features among sources to refine the multi-source fused features. In addition, to get rid of the inevitable interference caused by low-quality optical flow, we design a novel predictor selection network, which automatically chooses the results from static saliency predictor and moving object predictor. The automatic predictor selection network is simple yet effective, therefore, it can provide an important reference for other optical flow based methods. Extensive experiments on three ZVOS datasets indicate that the proposed method performs favorably against the current state-of-the-art methods.

ACKNOWLEDGMENTS

This work was supported in part by the National Natural Science Foundation of China #61876202, #61725202, #61751212 and #61829102, the Dalian Science and Technology Innovation Foundation #2019J12GX039, and the Fundamental Research Funds for the Central Universities #DUT20ZD212.

REFERENCES

- [1] Ning An, Xiao-Guang Zhao, and Zeng-Guang Hou. 2016. Online RGB-D tracking via detection-learning-segmentation. In *ICPR*. 1231–1236.
- [2] Jingchun Cheng, Yi-Hsuan Tsai, Shengjin Wang, and Ming-Hsuan Yang. 2017. Segflow: Joint learning for video object segmentation and optical flow. In *ICCV*. 686–695.
- [3] Yupeng Cheng, Huazhu Fu, Xingxing Wei, Jiangjian Xiao, and Xiaochun Cao. 2014. Depth enhanced saliency detection method. In *ICIMCS*. 23.
- [4] Pieter-Tjerk De Boer, Dirk P Kroese, Shie Mannor, and Reuven Y Rubinfeld. 2005. A tutorial on the cross-entropy method. *Annals of operations research* 134, 1 (2005), 19–67.
- [5] Jia Deng, Wei Dong, Richard Socher, Li-Jia Li, Kai Li, and Li Fei-Fei. 2009. Imagenet: A large-scale hierarchical image database. In *CVPR*. 248–255.
- [6] Muhammad Faisal, Ijaz Akhter, Mohsen Ali, and Richard Hartley. 2019. Exploiting geometric constraints on dense trajectories for motion saliency. *arXiv preprint arXiv:1909.13258* (2019).
- [7] Deng-Ping Fan, Zheng Lin, Jia-Xing Zhao, Yun Liu, Zhao Zhang, Qibin Hou, Menglong Zhu, and Ming-Ming Cheng. 2019. Rethinking RGB-D salient object detection: Models, datasets, and large-scale benchmarks. *arXiv preprint arXiv:1907.06781* (2019).
- [8] Kaiming He, Xiangyu Zhang, Shaoqing Ren, and Jian Sun. 2015. Delving deep into rectifiers: Surpassing human-level performance on imagenet classification. In *ICCV*. 1026–1034.
- [9] Kaiming He, Xiangyu Zhang, Shaoqing Ren, and Jian Sun. 2016. Deep residual learning for image recognition. In *CVPR*. 770–778.
- [10] Qibin Hou, Ming-Ming Cheng, Xiaowei Hu, Ali Borji, Zhuowen Tu, and Philip HS Torr. 2017. Deeply supervised salient object detection with short connections. In *CVPR*. 3203–3212.
- [11] Tak-Wai Hui, Xiaoou Tang, and Chen Change Loy. 2018. Liteflownet: A lightweight convolutional neural network for optical flow estimation. In *CVPR*. 8981–8989.
- [12] Suyog Dutt Jain, Bo Xiong, and Kristen Grauman. 2017. Fusionseg: Learning to combine motion and appearance for fully automatic segmentation of generic objects in videos. In *CVPR*. 2117–2126.
- [13] Yuan Ji, Xu Jia, Huchuan Lu, and Xiang Ruan. 2021. Weakly-Supervised Temporal Action Localization via Cross-Stream Collaborative Learning. In *ACMMM*.
- [14] Ran Ju, Ling Ge, Wenjing Geng, Tongwei Ren, and Gangshan Wu. 2014. Depth saliency based on anisotropic center-surround difference. In *ICIP*. 1115–1119.
- [15] Yeong Jun Koh and Chang-Su Kim. 2017. Primary object segmentation in videos based on region augmentation and reduction. In *CVPR*. 3442–3450.
- [16] Siyang Li, Bryan Seybold, Alexey Vorobyov, Xuejing Lei, and C-C Jay Kuo. 2018. Unsupervised video object segmentation with motion-based bilateral networks. In *ECCV*. 207–223.
- [17] Tsung-Yi Lin, Piotr Dollár, Ross Girshick, Kaiming He, Bharath Hariharan, and Serge Belongie. 2017. Feature pyramid networks for object detection. In *CVPR*. 2117–2125.
- [18] Hong Liu, Wenshan Wu, Xiangdong Wang, and Yueliang Qian. 2018. RGB-D joint modelling with scene geometric information for indoor semantic segmentation. *Multimedia Tools and Applications* 77, 17 (2018), 22475–22488.
- [19] Wei Liu, Andrew Rabinovich, and Alexander C Berg. 2015. Parsenet: Looking wider to see better. *arXiv preprint arXiv:1506.04579* (2015).
- [20] Xiankai Lu, Wenguan Wang, Chao Ma, Jianbing Shen, Ling Shao, and Fatih Porikli. 2019. See more, know more: Unsupervised video object segmentation with co-attention siamese networks. In *CVPR*. 3623–3632.
- [21] Alan Lukezic, Ugur Kart, Jani Kapyla, Ahmed Durmush, Joni-Kristian Kamarainen, Jiri Matas, and Matej Kristan. 2019. CDTB: A color and depth visual object tracking dataset and benchmark. In *ICCV*. 10013–10022.
- [22] Yuzhen Niu, Yujie Geng, Xueqing Li, and Feng Liu. 2012. Leveraging stereopsis for saliency analysis. In *CVPR*. 454–461.
- [23] Mertalp Ocal and Armin Mustafa. 2020. RealMonoDepth: Self-Supervised Monocular Depth Estimation for General Scenes. *arXiv preprint arXiv:2004.06267* (2020).
- [24] Peter Ochs, Jitendra Malik, and Thomas Brox. 2013. Segmentation of moving objects by long term video analysis. *IEEE TPAMI* 36, 6 (2013), 1187–1200.
- [25] Youwei Pang, Lihe Zhang, Xiaoqi Zhao, and Huchuan Lu. 2020. Hierarchical dynamic filtering network for RGB-D salient object detection. In *ECCV*. 235–252.
- [26] Youwei Pang, Xiaoqi Zhao, Lihe Zhang, and Huchuan Lu. 2020. Multi-Scale Interactive Network for Salient Object Detection. In *CVPR*. 9413–9422.
- [27] Anestis Papazoglou and Vittorio Ferrari. 2013. Fast object segmentation in unconstrained video. In *ICCV*. 1777–1784.
- [28] Houwen Peng, Bing Li, Weihua Xiong, Weiming Hu, and Rongrong Ji. 2014. RGBD salient object detection: A benchmark and algorithms. In *ECCV*. 92–109.
- [29] Federico Perazzi, Jordi Pont-Tuset, Brian McWilliams, Luc Van Gool, Markus Gross, and Alexander Sorkine-Hornung. 2016. A benchmark dataset and evaluation methodology for video object segmentation. In *CVPR*. 724–732.
- [30] Yongri Piao, Wei Ji, Jingjing Li, Miao Zhang, and Huchuan Lu. 2019. Depth-Induced Multi-Scale Recurrent Attention Network for Saliency Detection. In *ICCV*. 7254–7263.
- [31] Sudeep Pillai, Rareş Ambruş, and Adrien Gaidon. 2019. Superdepth: Self-supervised, super-resolved monocular depth estimation. In *ICRA*. 9250–9256.
- [32] Alessandro Presti, Christian Leistner, Javier Civera, Cordelia Schmid, and Vittorio Ferrari. 2012. Learning object class detectors from weakly annotated video. In *CVPR*. 3282–3289.
- [33] Xuebin Qin, Zichen Zhang, Chenyang Huang, Chao Gao, Masood Dehghan, and Martin Jagersand. 2019. BASNet: Boundary-Aware Salient Object Detection. In *CVPR*. 7479–7489.
- [34] René Ranftl, Katrin Lasinger, David Hafner, Konrad Schindler, and Vladlen Koltun. 2020. Towards robust monocular depth estimation: Mixing datasets for zero-shot cross-dataset transfer. *IEEE TPAMI* (2020).
- [35] Anurag Ranjan and Michael J Black. 2017. Optical flow estimation using a spatial pyramid network. In *CVPR*. 4161–4170.
- [36] Maryamsadat Rasoulidaneh, Srishti Yadav, Sachini Herath, Yasaman Vaghei, and Shahram Payandeh. 2019. Deep Attention Models for Human Tracking Using RGBD. *Sensors* 19, 4 (2019), 750.
- [37] Mennatullah Siam, Chen Jiang, Steven Lu, Laura Petrich, Mahmoud Gamal, Mohamed Elhoseiny, and Martin Jagersand. 2019. Video object segmentation using teacher-student adaptation in a human robot interaction (hri) setting. In *ICRA*. 50–56.
- [38] Hongmei Song, Wenguan Wang, Sanyuan Zhao, Jianbing Shen, and Kin-Man Lam. 2018. Pyramid dilated deeper convlstm for video salient object detection. In *ECCV*. 715–731.
- [39] D Sun, X Yang, MY Liu, and J Kautz. 2018. PWC-Net: CNNs for Optical Flow Using Pyramid, Warping, and Cost Volume. In *CVPR*. 8934–8943.
- [40] Zachary Teed and Jia Deng. 2020. Raft: Recurrent all-pairs field transforms for optical flow. In *ECCV*. 402–419.
- [41] Pavel Tokmakov, Karteek Alahari, and Cordelia Schmid. 2017. Learning motion patterns in videos. In *CVPR*. 3386–3394.
- [42] Pavel Tokmakov, Karteek Alahari, and Cordelia Schmid. 2017. Learning video object segmentation with visual memory. In *ICCV*. 4481–4490.
- [43] Yi-Hsuan Tsai, Guangyu Zhong, and Ming-Hsuan Yang. 2016. Semantic co-segmentation in videos. In *ECCV*. 760–775.
- [44] Tiantian Wang, Lihe Zhang, Shuo Wang, Huchuan Lu, Gang Yang, Xiang Ruan, and Ali Borji. 2018. Detect globally, refine locally: A novel approach to saliency detection. In *CVPR*. 3127–3135.
- [45] Wenguan Wang, Xiankai Lu, Jianbing Shen, David J Crandall, and Ling Shao. 2019. Zero-shot video object segmentation via attentive graph neural networks. In *ICCV*. 9236–9245.
- [46] Weiyue Wang and Ulrich Neumann. 2018. Depth-aware cnn for rgb-d segmentation. In *ECCV*. 135–150.
- [47] Wenguan Wang, Jianbing Shen, and Fatih Porikli. 2015. Saliency-aware geodesic video object segmentation. In *CVPR*. 3395–3402.
- [48] Wenguan Wang, Hongmei Song, Shuyang Zhao, Jianbing Shen, Sanyuan Zhao, Steven CH Hoi, and Haibin Ling. 2019. Learning unsupervised video object segmentation through visual attention. In *CVPR*. 3064–3074.
- [49] Zhou Wang, Eero P Simoncelli, and Alan C Bovik. 2003. Multiscale structural similarity for image quality assessment. In *The Thirty-Seventh Asilomar Conference on Signals, Systems & Computers, 2003*, Vol. 2. 1398–1402.
- [50] Gengshan Yang and Deva Ramanan. 2019. Volumetric correspondence networks for optical flow. In *Advances in neural information processing systems*. 794–805.
- [51] Lu Zhang, Jianming Zhang, Zhe Lin, Radomir Mech, Huchuan Lu, and You He. 2020. Unsupervised Video Object Segmentation with Joint Hotspot Tracking. In *ECCV*. 490–506.
- [52] Pingping Zhang, Dong Wang, Huchuan Lu, Hongyu Wang, and Xiang Ruan. 2017. Amulet: Aggregating multi-level convolutional features for salient object detection. In *ICCV*. 202–211.
- [53] Zhenyu Zhang, Zhen Cui, Chunyan Xu, Yan Yan, Nicu Sebe, and Jian Yang. 2019. Pattern-affinitive propagation across depth, surface normal and semantic segmentation. In *CVPR*. 4106–4115.
- [54] Jiawei Zhao, Yifan Zhao, Jia Li, and Xiaowu Chen. 2020. Is depth really necessary for salient object detection?. In *ACMMM*. 1745–1754.
- [55] Shengyu Zhao, Yilun Sheng, Yue Dong, Eric I Chang, Yan Xu, et al. 2020. Mask-Flownet: Asymmetric Feature Matching with Learnable Occlusion Mask. In *CVPR*. 6278–6287.
- [56] Xiaoqi Zhao, Youwei Pang, Lihe Zhang, Huchuan Lu, and Lei Zhang. 2020. Suppress and balance: A simple gated network for salient object detection. In *ECCV*. 35–51.
- [57] Xiaoqi Zhao, Lihe Zhang, Youwei Pang, Huchuan Lu, and Lei Zhang. 2020. A single stream network for robust and real-time rgb-d salient object detection. In *ECCV*. 646–662.
- [58] Mingmin Zhen, Shiwei Li, Lei Zhou, Jiayang Shang, Haoan Feng, Tian Fang, and Long Quan. 2020. Learning Discriminative Feature with CRF for Unsupervised Video Object Segmentation. In *ECCV*. 445–462.
- [59] Tianfei Zhou, Shunzhou Wang, Yi Zhou, Yazhou Yao, Jianwu Li, and Ling Shao. 2020. Motion-Attentive Transition for Zero-Shot Video Object Segmentation.. In *AAAI*. 3.